

Real-Time Monitoring of Crack Propagation in Fiber-Reinforced Composite Plates using iFEM Methodology

A. Kefal, I.E. Tabrizi & M. Yildiz

Faculty of Engineering and Natural Sciences, Sabanci University, Istanbul, Turkey

Integrated Manufacturing Technologies Research & Application Center, Sabanci University, Istanbul, Turkey

Composite Technologies Center of Excellence, Sabanci University-Kordsa, Istanbul, Turkey

ABSTRACT: Inverse finite element method (iFEM) is an efficient and robust approach to obtain displacement/strain/stress state of the structure by monitoring strain values obtained from discrete locations in the structure. Therefore, the iFEM methodology can precisely detect any variation in strain field of the structure due to presence of damages inside the material. In this study, the advantage of using iFEM methodology for monitoring crack propagation in a laminated composite is shown for the first time in the literature. To this end, a pre-cracked composite plate is loaded under tensile loading condition and crack growth is monitored using digital image correlation (DIC) system. The discrete strain data obtained from DIC are used as an input for the iFEM algorithm, and full field displacements/strains are reconstructed using an inverse-plane element formulation. This full field information is leveraged to predict an exact crack length and monitor its dynamic propagation until the global failure of the material. The iFEM methodology demonstrates an unprecedented precision in crack growth monitoring inside the composite laminate without necessity of previous knowledge about material properties and the position of the initial damages/cracks.

1 INTRODUCTION

Fiber reinforced polymer matrix materials are used in marine structures due to their high specific strength and corrosion resistance properties. Nevertheless, gradual damage accumulation inside these composite materials followed by abrupt failure is a challenging problem for a long time. Rapid growth of cracks in marine structures such as submarine hulls and navy vessels can result in catastrophic failure of the structure. Therefore, design engineers are required to study details of the crack dynamics via numerical tools and validate the numerical results with that of experimental analysis. For such experimental test, on-board structural health monitoring systems have been extensively utilized either on test-and/or real-scale of marine structures (Kefal, 2017, Silva-Muñoz & Lopez-Anido, 2009). These tools can provide valuable real-time data about stiffness degradation and concurrent displacement and stress monitoring of marine structures, e.g., shape sensing in laminated composite structures (Kefal et al., 2021a).

Different shape sensing methods have been introduced over the years, namely Ko's displacement theories (Ko et al., 2009), modal based algorithms (Kim & Cho, 2004), artificial neural network algorithms (Moreira & Soares, 2020, Bruno et al., 1994, Glaser et al., 2012), and inverse finite element meth-

od (iFEM) (Tessler & Spangler, 2005). Recent studies have shown that iFEM methodology provides the most robust and reliable shape-sensing results as compared to other algorithms (Gherlone et al., 2018, Abdollahzadeh et al., 2020, Esposito et al., 2020). The iFEM approach does not require any information about loading and material properties. Moreover, it is insensitive to noise that may be available in experimental measurement. Furthermore, it can be used for complex boundary conditions and structural topologies. As a result, the iFEM methodology fulfills all requirements of a reliable SHM system for marine structures (Kefal et al., 2018).

Since the development of original iFEM formulation (Tessler & Spangler, 2005), numerous studies have investigated the performance of iFEM methodology using new C^0 -continuous inverse-shell elements, namely three-node triangular inverse-shell element (iMIN3) (Tessler & Spangler, 2004), four-node quadrilateral inverse-shell element (iQS4) (Kefal et al., 2016), and eight-node curved quadrilateral inverse-shell element (iCS8) (Kefal, 2019). Moreover, iFEM has been combined with high-order shear deformation theories such as refined zigzag theory (Tessler et al., 2010) to predict the precise deformation field in laminated plate (Cerracchio et al., 2015), shell (Kefal et al., 2017), and beam (Zhao et al., 2021) structures. Several studies have shown the application of iFEM/iQS4 approach for shape sens-

ing and damage prediction of cylindrical marine structures (Li et al., 2020a), submarine pressure hulls (Li et al., 2019), monolithic/stiffened engineering structures (Colombo et al., 2019, Colombo et al., 2021, Roy et al., 2021, Oboe et al., 2021), merchant vessels including Panamax container ships (Kefal & Oterkus, 2016) and offshore wind turbines (Li et al., 2020b). Recently, a novel approach named as smoothed inverse finite element method (iFEM^(s)) has been developed to obtain continuous strain fields from discrete strain measurement and subsequently integrate this information with iFEM for shape sensing of the structure (Kefal et al., 2021b). It was revealed that iFEM^(s) methodology can provide more accurate shape sensing results as compared to conventional iFEM approaches. Despite all these efforts, the application of iFEM in damage/crack propagation analysis of isotropic/composite materials is still unexplored. Coupling the iFEM tool with conventional SHM systems can be beneficial to understand crack growth dynamics in engineering structures by leveraging the full-field deformations/strains reconstructed by iFEM.

Usage of SHM techniques as a tool for failure analysis in composite materials has been established for decades. Researcher have used methods such as acoustic emission, digital image correlation (DIC), infrared thermography, and fiber Bragg grating sensors individual (Tabrizi et al., 2019a, Massarwa et al. 2021) or combined (Ali et al., 2019, Tabrizi et al., 2019b) manner to understand the specific damage mode and its accumulation under various loading conditions in fiber reinforced laminates and sandwich structures. Among the methods mentioned above, with the ability to provide local and global displacement field as discrete point clouds, the DIC system has become ever more appealing for failure analysis, thereby lending itself to become one of the most popular noncontact measurement systems (AlKhateab et al., 2020, Khan et al., 2020). Nevertheless, combined usage of DIC with novel iFEM techniques has not been investigated thoroughly in the literature yet.

The main aim of this study is to demonstrate the capability of iFEM formulation as a robust real-time approach for prediction of the crack growth in composite laminates. To do so, the point-wise strain data collected via DIC for a pre-cracked woven carbon fabric composite under tensile loading condition is used as an input for iFEM algorithm. Then, the discrete strain data is processed by utilizing a two-dimensional inverse-plane element, and full-field displacements are obtained over the geometry of tensile specimen. Accordingly, the reconstructed displacement maps from inverse analysis are validated by making comparisons against DIC displacement maps. Moreover, the continuous strain field obtained by taking derivatives of the reconstructed displacements are utilized to quantify the

crack propagation. The attained results reveal that despite lack of experimental data at failure point of the laminate, due to very rapid crack growth, the iFEM methodology can successfully circumvent this issue and monitor crack growth in real time. Overall, it is shown that iFEM technique is a viable SHM technology for crack detection and monitoring of its growth in composite structures.

2 THE INVERSE FINITE ELEMENT FORMULATION FOR TWO DIMENSIONAL STRUCTURES

In this section, the mathematical formulation of iFEM methodology is presented for shape sensing or displacement monitoring analysis of a two-dimensional solid structure. Consider that this plate geometry represents either orthotropic laminate or isotropic plate and is located within a Cartesian global coordinate system $(x, y, z) \equiv (\mathbf{x}, z)$ as depicted in Figure 1. The thickness dimension, h , here is assumed to be very small as compared to other dimensions of the plate, and plate is subjected to only in-plane tractions, t_x , while being constraint from one of its edges.

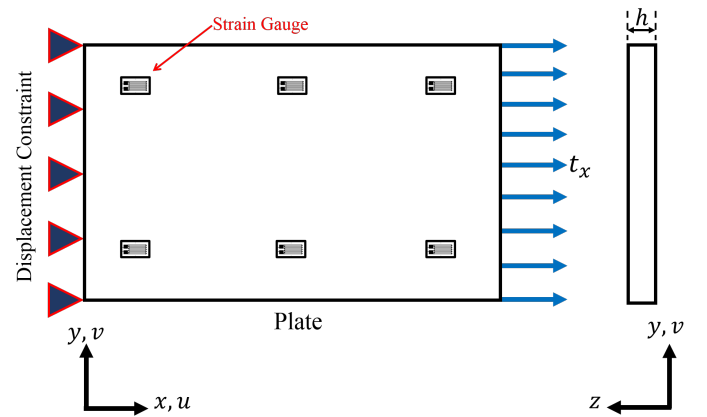


Figure 1. Inverse problem of a two-dimensional solid.

Under such mechanical condition, plate structure can be modelled as a plane stress problem of a two dimensional solid. Accordingly, one can adopt single-layer representation and express the displacement components of a material point within the plate as:

$$\mathbf{u}(x, y) \equiv \begin{Bmatrix} u(x, y) \\ v(x, y) \end{Bmatrix} \quad (1)$$

where the u and v represent the translational displacements along global coordinates of x and y , respectively, as shown in Figure 1. Here, the $\mathbf{u} = \mathbf{u}(\mathbf{x})$ vector contains these translational kinematic variables, which are the main unknowns of present inverse problem.

According to linear elasticity, the small strains can be established through taking derivatives of displacement components as:

$$\boldsymbol{\varepsilon} \equiv \begin{Bmatrix} \varepsilon_{xx} \\ \varepsilon_{yy} \\ \gamma_{xy} \end{Bmatrix} = \begin{bmatrix} \frac{\partial u}{\partial x} & \frac{\partial v}{\partial y} & \frac{\partial v}{\partial x} + \frac{\partial u}{\partial y} \end{bmatrix}^T \quad (2a)$$

$$\varepsilon_{zz} = \gamma_{xz} = \gamma_{yz} = 0 \quad (2b)$$

where the vector $\boldsymbol{\varepsilon}$ represents the in-plane strains with ε_{xx} , ε_{yy} , γ_{xy} being the normal strains along x , and y axes and shear angle in the xy -plane, in the given order. Since the thickness coordinate in the present iFEM formulations is not concerned, the strains associated with the third dimension are set to zero as given in Eq. (2b). The iFEM formulation requires a suitable discretization of the geometrical domain by using inverse-elements. Then, for each element domain, the kinematic variables can be interpolated through relevant linear/quadratic shape functions. For the present geometry, we use a four-node inverse-plane element and approximate the displacement components as:

$$u = \sum_{i=1}^4 N_i u_i = N_1 u_1 + \dots + N_4 u_4 \quad (3a)$$

$$v = \sum_{i=1}^4 N_i v_i = N_1 v_1 + \dots + N_4 v_4 \quad (3b)$$

where N_i represents the bilinear isoparametric shape functions, and (u_i, v_i) is the nodal displacement degrees-of-freedom (DOF) along the global Cartesian coordinates. For the notational clarity, the Eq. (3) can be written in the compact matrix-vector form as:

$$\mathbf{u} = \mathbf{N} \mathbf{u}^e \quad (4a)$$

$$\mathbf{N} = [\mathbf{N}_1 \quad \dots \quad \mathbf{N}_4], \quad \mathbf{N}_i = \begin{bmatrix} N_i & 0 \\ 0 & N_i \end{bmatrix} \quad (4b)$$

where \mathbf{N} matrix is the shape function matrix of the inverse-plane element and \mathbf{u}^e is the nodal DOF vector of the element, which can be defined as:

$$\mathbf{u}^e = [\mathbf{u}_1^e \quad \dots \quad \mathbf{u}_4^e]^T, \quad \mathbf{u}_i^e = \begin{Bmatrix} u_i \\ v_i \end{Bmatrix} \quad (4c)$$

Substituting the shape function matrix of the element into the Eq. (2a), the strains can be defined over an element domain as:

$$\boldsymbol{\varepsilon} = \mathbf{B} \mathbf{u}^e \quad (5a)$$

$$\mathbf{B} = [\mathbf{B}_1 \quad \dots \quad \mathbf{B}_4], \quad \mathbf{B}_i = \begin{bmatrix} N_{i,x} & 0 \\ 0 & N_{i,y} \\ N_{i,y} & N_{i,x} \end{bmatrix} \quad (5b)$$

where the \mathbf{B} matrix establishes the strain-displacement relations within the element domain through the derivatives of the shape functions, i.e.,

$N_{i,x}$ and $N_{i,y}$. These derivatives can be readily calculated using the chain rule definitions of the classical finite element formulations provided that the isoparametric formulation is used to define the shape functions. Otherwise, these derivatives can be directly taken without the need of Jacobian mapping.

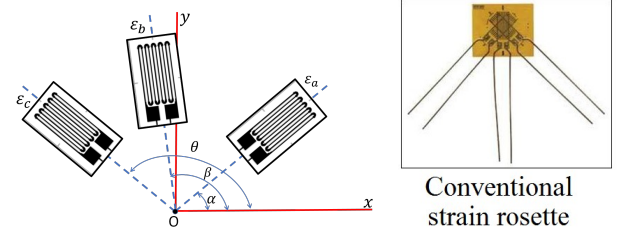


Figure 2. Experimental strain gauge measurement.

In practice, the iFEM methodology reconstruct the displacement field of a given geometry by using the experimentally measured section strains. The present inverse problem will have identical strain maps on top and bottom surfaces of the plate. Therefore, unlike classical iFEM formulations, the experimental input from either top/bottom surface of the plate would be adequate to account for experimental counterparts of the in-plane strains, $\boldsymbol{\varepsilon}$. To this end, as depicted in Figure 2, the surface strain gauges can be mounted on the top/bottom surfaces of the plate, providing the triaxial strain measurements at the position of \mathbf{x}_i ($i=1,2,\dots,n$). Using the relevant strain transformation equations according to the orientation of each strain gauges in the rosette, the experimental strains along the global coordinates can be calculated as:

$$\varepsilon_a = \frac{e_{xx} + e_{yy}}{2} + \frac{e_{xx} - e_{yy}}{2} \cos 2\alpha + \frac{e_{xy}}{2} \sin 2\alpha \quad (6a)$$

$$\varepsilon_b = \frac{e_{xx} + e_{yy}}{2} + \frac{e_{xx} - e_{yy}}{2} \cos 2\beta + \frac{e_{xy}}{2} \sin 2\beta \quad (6b)$$

$$\varepsilon_c = \frac{e_{xx} + e_{yy}}{2} + \frac{e_{xx} - e_{yy}}{2} \cos 2\theta + \frac{e_{xy}}{2} \sin 2\theta \quad (6c)$$

where the symbols $\varepsilon_a, \varepsilon_b, \varepsilon_c$ denote the experimental strains measured along the axial directions having positive α, β, θ angle difference with respect to the global x coordinate. The e_{xx}, e_{yy}, e_{xy} in the Eq. (6) represent the experimental in-plane strains, i.e., experimental counterparts of $\varepsilon_{xx}, \varepsilon_{yy}, \gamma_{xy}$ strains. These in situ values can be directly obtained by solving the Eq. (6) for any strain-data acquisition from the strain gauges. For example, consider that a strain rosette is patched on the surface of a structure with the $(\alpha, \beta, \theta) = (0, 45, 90)$ orientations in the real test environment, then the explicit values of experimental in-plane strains can be computed as:

$$\mathbf{e} = [e_{xx} \quad e_{yy} \quad e_{xy}]^T = [\varepsilon_a \quad \varepsilon_c \quad 2\varepsilon_b - \varepsilon_a - \varepsilon_c]^T \quad (7)$$

After the strains are experimentally obtained at discrete positions, they can be smoothed *'a priori'* to increase the fidelity of the experimental strain maps, thereby yielding a higher accuracy of the displacement reconstruction based on iFEM methodology. For this purpose, one can employ the similar logic of iFEM^(s) methodology (Kefal et al., 2021b), which explicitly demonstrates the implementation of the smoothing element algorithm (Tessler et al., 1999) to various iFEM formulations. Accordingly, the *'i'* subscript representing the discreteness of the experimental strains is dropped hereafter for mathematical simplicity, and it is assumed that the experimental strains are available everywhere within the two-dimensional structural domain.

The iFEM methodology defines a weighted-least-squares functional to correlate the individual analytical strains with their experimental counterparts as:

$$\Phi \equiv \Phi(\mathbf{u}^e) = \frac{1}{A} \iint_A w \|\boldsymbol{\varepsilon}(\mathbf{u}^e) - \mathbf{e}\|^2 dx dy \quad (8)$$

where the A and w terms represent the area and weighting constant of an inverse-plane element, respectively. The w constant is positive weight that controls the strain-interpolation connectivity between the elements having strain-gauge measurements. If an inverse-element has experimental strain, the weighting coefficient is set to 1. On the other hand, it can be set to a small number (e.g., $w = 10^{-3}$) as compared to unity for an inverse-element having no sensors. Substituting the Eq. (5a) into Eq. (8), the Φ functional can be written as:

$$\Phi = \frac{w}{A} \iint_A (\mathbf{u}^{eT} \mathbf{B}^T \mathbf{B} \mathbf{u}^e - 2\mathbf{u}^{eT} \mathbf{B}^T \mathbf{e} + \mathbf{e}^T \mathbf{e}) dx dy \quad (9a)$$

which can be subsequently minimized with respect to unknown displacement DOF as:

$$\frac{\partial \Phi(\mathbf{u}^e)}{\partial \mathbf{u}^e} = \frac{w}{A} \iint_A 2(\mathbf{B}^T \mathbf{B} \mathbf{u}^e - \mathbf{B}^T \mathbf{e}) dA = 0 \quad (9b)$$

Such minimization yields to the final set of iFEM matrix-vector equations as:

$$\mathbf{k}^e \mathbf{u}^e = \mathbf{f}^e \quad (10a)$$

$$\mathbf{k}^e = \frac{w}{A} \iint_A \mathbf{B}^T \mathbf{B} dA \quad (10b)$$

$$\mathbf{f}^e = \frac{w}{A} \iint_A \mathbf{B}^T \mathbf{e} dA \quad (10c)$$

where \mathbf{k}^e matrix is calculated once with no further update required during monitoring process, whereas \mathbf{f}^e is a function of experimental strains, thus its recalculation is necessary for each strain-data update in real time. After constructing the local (element) equations, they can be assembled to obtain global

matrix-vector system of the whole discretization. This assembly process can be realized like that of conventional finite element method. Finally, problem-specific constraint boundary conditions can be applied to the global matrix-vector equations and subsequently solved for predicting structural deformed shape at any real-time.

3 PREPARATION OF TEST SETUP

A laminated composite plate with a center crack is experimentally tested under tensile loading condition. During this test, strain data is collected at discrete points by using DIC system. This data is directly used as an input to the inverse analysis to demonstrate the monitoring capabilities of the iFEM methodology for a propagating crack in the specimen. To this end, the detailed distributions of the displacements and strains reconstructed from sensor (DIC) measurements by using iFEM are quantitatively examined and presented in the next section. This section continues with the detailed explanation of specimen preparation, and test setup for DIC strain-data acquisition from the composite laminate.

To manufacture the composite laminates, 2×2 twill fabric with T300 type carbon fibers and 245 gsm were used. A two components resin system from Sika with product names of Biresin CR122 and CH122-3 were used as matrix. The resin system had a mixed viscosity of 370 mPa.s at room temperature and glass transition of 114°C. CFRP laminates were manufactured using vacuum assisted resin transfer molding (VARTM) using the following procedure. Total of 8 fabrics were cut with the size of 300mm×600mm and stacked upon a clean and dry mold that had been prepared using three layers of sealer (XTEND 838) and releaser (XTEND CX-500) agents in sequence with 20 min of time intervals. Cut fabrics were covered with peel ply, bleeder fabric and flow mesh in the given order. Spiral pipes were utilized as vacuum outlet and resin inlet and placed parallel to the length of the woven fabrics at two sides of the setup.

Vacuum bag was laid on the whole set up and sealed from the edges of the mold using tacky tape. The resin system was prepared with the mass ratio of 10 to 3 for epoxy and hardener, respectively, and degassing procedure was implemented to minimize air entrapment inside the composite structure after manufacturing. Afterwards, the resin was fully infused into the mold and wetting of all fabrics was accomplished. The system was cured at room temperature for 48h before demolding. The cured laminate was cut using water jet to obtain rectangular samples with the size of 200mm×75mm and a mid-plane transverse crack with the length of 18.7 mm as seen in Figure 3. Moreover, glass fiber reinforced laminates with $[\pm 45]_{2s}$ layup and the size of 25mm×75mm were adhered as tab at both ends of

the specimens. Therefore, the gauge length of the tensile sample becomes 150mm after tabbing.

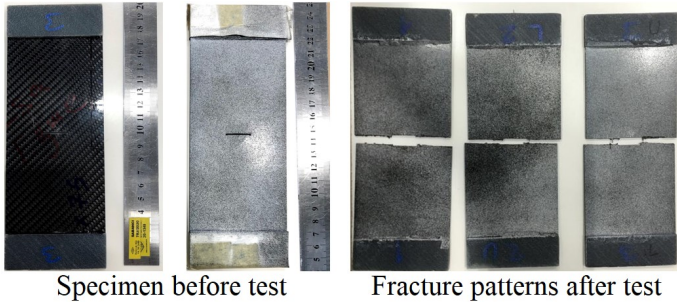


Figure 3. Composite specimens before and after tensile test.

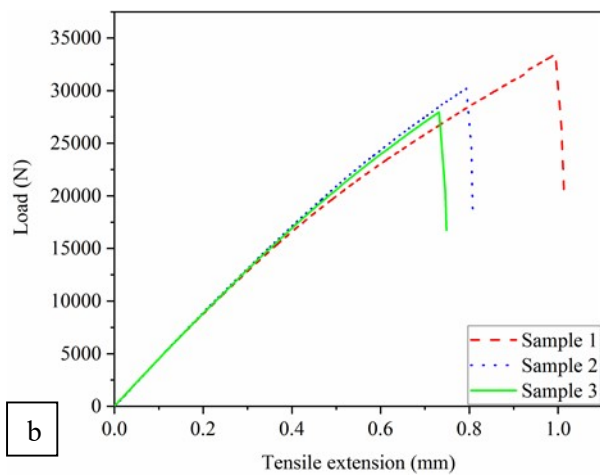
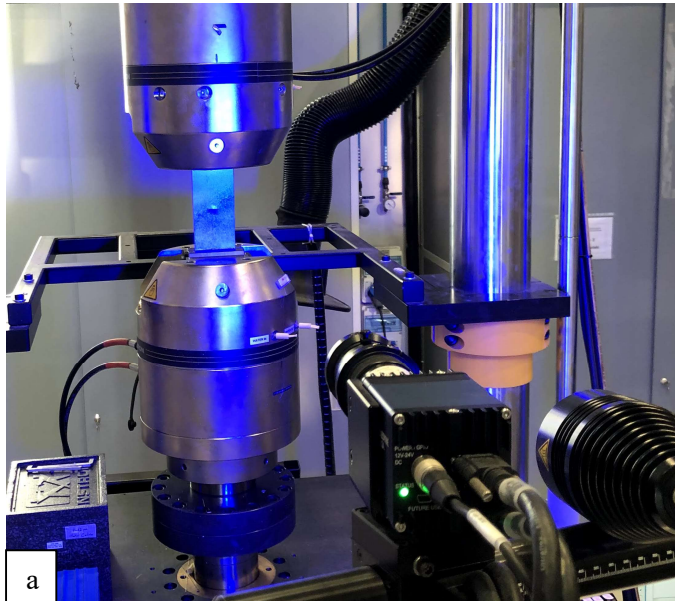


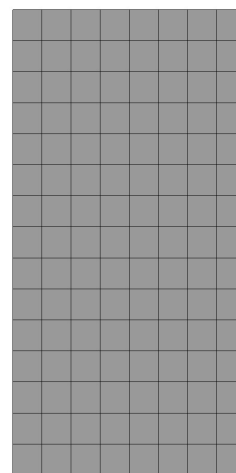
Figure 4. a) Tensile test setup with DIC measurements, b) displacement-force plots for tested samples.

As illustrated in Figure 3, random speckle pattern was applied on one side to the samples to prepare a high contrast region detectable with DIC sensors during deformation. The tensile tests were conducted at constant speed of 2mm/min and the relevant surface of the laminate was monitored using calibrated 2D-DIC setup as shown in Figure 4a. The post processing of obtained images with DIC was accomplished with GOM Correlate software using a facet size of 25 pixels and step size of 19 pixels. The tensile test was repeated for the 3 tensile specimens to

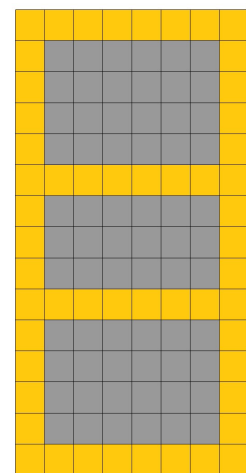
minimize any possible experimental error in the crack propagation. The force-displacement plots for tested specimen is given in Figure 4b. Accordingly, the final fracture patterns are very similar for all three composite samples as shown in Figure 3, thereby proving the accuracy and repeatability of the performed experimental tests. All the DIC strain data collected within these test periods are averaged between samples. Afterwards, these discrete DIC strains are utilized to generate input data (namely, experimental strain data collected from sensors at discrete points) for reconstruction of displacements based on iFEM technique.

4 EXPERIMENTAL AND NUMERICAL RESULTS

Since the obtained discrete strain data from DIC measurements (experimental strain) can be used as an input for iFEM model to reconstruct the full field displacements, one can readily use the DIC strain values and treat them as the collected data from resistive strain gauge sensors at various locations on the surface of the material. Thus, the achieved full field displacement contour from iFEM analysis can be compared to that of DIC results for validation. Various sensor placement configurations with different density and alignment of strain gauges can be chosen to examine the ability of iFEM in prediction of crack growth dynamics in composite plate structures. The details about the strategy for optimizing the number and configuration of sensors can be found in the recent study of Kefal & Yildiz (2017).



Model-1: All inverse-elements have sensor



Model-2: Only yellow inverse-elements have sensor

Figure 5. Sensor configurations for iFEM analysis

As seen in Figure 5, we have used two sensor patterns (sampling locations of DIC strain), namely full sensor pattern (Model-1) with 15×8 inverse elements and sparse sensor pattern (Model-2). In the full sensor pattern, all the inverse-plane elements have a strain rosette positioned at their centroid whereas the sparse configuration (Model-2) only uses the strain

data collected from the centroid of yellow inverse elements. It must be noted that none of these iFEM models considers the presence of crack in the laminate, and no data regarding discontinuity in the middle of specimen are provided as an input to the iFEM domains.

Once the discrete strain sensor data obtained from DIC are analyzed using the iFEM algorithm, the full field displacements are reconstructed for the laminate at pre-failure, failure, and post failure moments as seen in Figure 6 and compared to that of DIC output at same time steps under identical loading conditions. Comparison of contour plots for DIC, iFEM (Model-1) and (Model-2) reveal a good consistency between the overall displacement gradient at pre-failure moment.

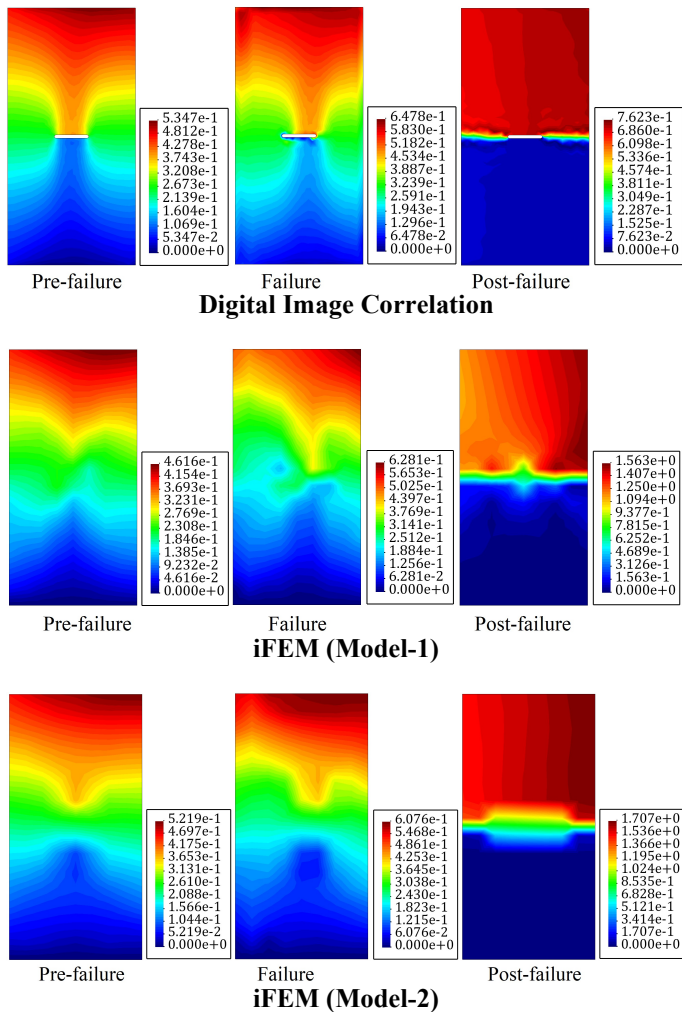


Figure 6. Comparison of total displacement contours predicted by DIC and iFEM analyses (Models 1-2).

The DIC displacement map at pre-failure stage is symmetrical with respect to the midplane of the specimen and iFEM analysis has appropriately reconstructed similar displacement field using discrete strain values obtained from individual locations on the surface of the laminate. It is seen that the maximum values for displacement prior to failure are 0.53mm, 0.46mm, and 0.52mm for DIC, Models 1-2, respectively. These results show difference of 13% and 2% as compared to DIC output for Models

1-2, respectively. It is remarkable to see that iFEM analysis has provided a consistent displacement result with negligible differences as compared to experimental measurements, despite having no prior crack information in the material.

The full field displacement map obtained from DIC at failure moment shows a maximum value of 0.64mm, while the full sensor pattern and sparse sensor configuration predict values of 0.62mm and 0.60mm, respectively. Thus, the shape sensing values at failure moment are 3% and 6% different from experimental results for Models 1-2, which again validate the superior shape-sensing capability of iFEM. A similar observation is obtained for post-failure step where the developed transverse crack has separated two segments of the laminated material. As seen in DIC displacement contour, the material is split into two sections where the lower half has the minimum and the upper piece has the maximum displacement values. The iFEM approach has successfully projected such a displacement field despite having no crack information. Moreover, it is evident that the iFEM analysis has also predicted the crack growth path throughout the width of sample after failure.

Once the full field displacement contours are reconstructed using iFEM analysis, the continuous strain maps for the same domain can be achieved straightaway. The reconstructed displacements can be used to calculate strain data such as principal strains, maximum shear strains, and equivalent von mises strains. Among these strain data, von Mises strain monitoring can be used to signify the regions of material with meaningful damage and thereby reveal the damage progress routes.

In Figure 7, the raw images taken via DIC for pre-failure, failure and post-failure steps are presented and compared with von Mises strain maps analyzed based on full sensor and sparse sensor patterns. The calculated maps based on Models 1-2 show maximum von Mises strains of 5000 $\mu\epsilon$ and 7650 $\mu\epsilon$, respectively at pre-failure stage. The highest strain values in both cases are in the middle of the sample where the transverse crack is located. Although no previous information about discontinuities in the material were provided for iFEM, the high strain gradient regions in the strain maps indicate significant damage presence at the middle of the laminate. As seen in Figure 7 for both models an apparent symmetry in von Mises strain maps is observed under uniaxial loading condition. The symmetry in full field strain map demonstrates the capability of iFEM approach to detect the shape of the damage inside the laminate.

The raw image at failure moment under uniaxial tensile loading shows the growth of crack in transverse direction in the middle of the sample. The continuous von Mises strain maps (i.e., obtained from iFEM analyses) related to failure moment are also

presented in Figure 7. When compared to pre-failure stage, the symmetry in full field strain contour is not seen for both full sensor and sparse sensor models. The sudden variation in strain map indicates growth of damage and creation of unbalanced crack growth in transverse direction which is observed in raw image as well. The maximum von Mises strain value for Model-1 shows an increase up to $10,000\mu\epsilon$ which is twice as much for pre-failure step. On the other hand, the difference between maximum values of pre-failure and failure moments using Model-2 is $2000\mu\epsilon$.

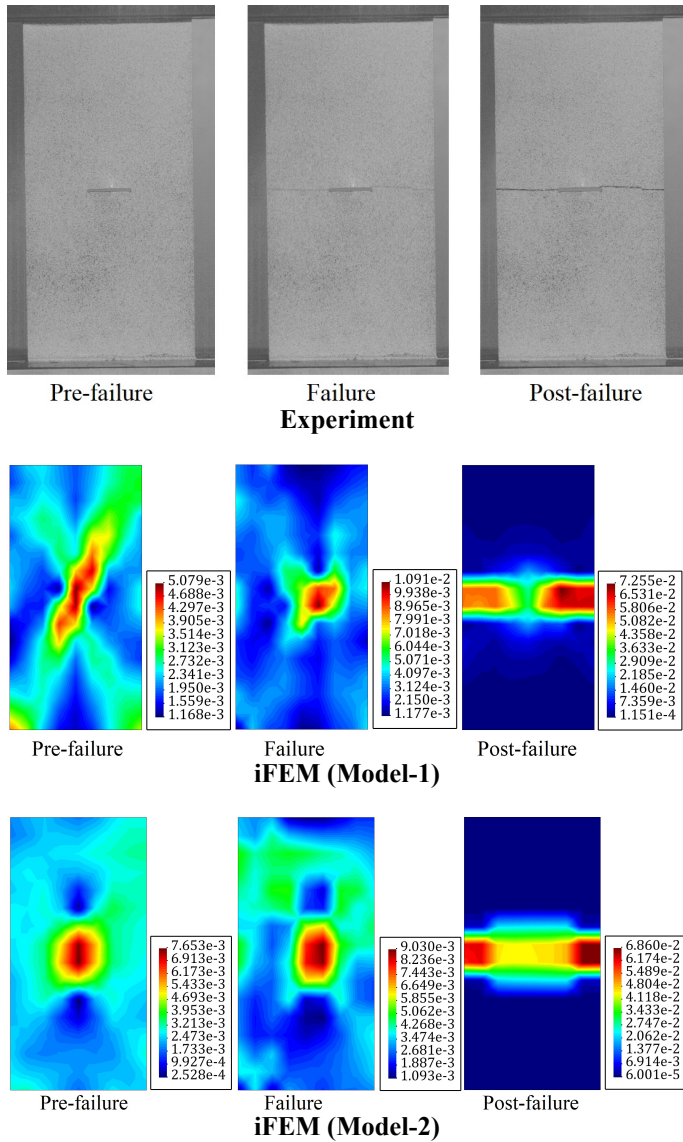


Figure 7. Crack propagation monitoring using von Mises strains predicted by iFEM analysis (Models 1-2) and its comparison with experiment.

The post-failure strain maps presented in Figure 7 show that the material has been separated into two segments signifying no deformation above and below the transverse crack. The split of material into two parts is also indicating the complete crack development path under tensile loading condition. The strain maps attained from displacement fields show the ability of iFEM for predicting apparent shape,

location, and development path of cracks inside the loaded laminate.

5 CONCLUSION

This study presented a successful application of iFEM methodology in real-time monitoring of damage growth inside laminated composite material. The formulation of iFEM methodology for two dimensional structures such as orthotropic laminate or isotropic plate is developed and the experimental test setup for manufacturing, mechanical loading and full field strain measurements are explained in detail. The discrete experimental strains are used as input for two sensor patterns. Even though no information about transverse crack in the sample was provided for iFEM, this method successfully reconstructed the full field displacement fields in the laminated composite at three stages namely, pre-failure, failure, and post-failure. In each sensor model, the displacement values had negligible differences (less than 5% in average) as compared to that of experimental DIC measurements.

The full field von Mises strain maps were calculated from full field displacement results of iFEM. The von Mises strain maps reveal presence of high strain gradients at damaged areas of the laminate and provide information about the apparent size and shape of the in-plane crack. The post failure analysis of von Mises strain maps show that the laminate has been divided into two segments where the path of crack development is clearly observed in between the sections. These results show that the usage of iFEM as a shape sensing technique can enable real-time monitoring of crack dynamics inside woven fabric reinforced laminates. Overall, the findings of this study show the high potential of iFEM approach for real-time shape sensing and damage/crack propagation monitoring inside engineering structures.

6 ACKNOWLEDGEMENT

The financial support provided by the Scientific and Technological Research Council of Turkey (TUBITAK) under the grant No: 217M207 is greatly acknowledged.

7 REFERENCES

- Abdollahzadeh, M.A., Kefal, A., & Yildiz, M., 2020. A comparative and review study on shape and stress sensing of flat/curved shell geometries using C^0 -continuous family of iFEM elements. *Sensors*, 20(14), p. 3808.
- Ali, H.Q., Tabrizi, I.E., Khan, R.M.A., Tufani, A., & Yildiz, M., 2019. Microscopic analysis of failure in woven carbon fabric laminates coupled with digital image correlation and acoustic emission. *Composite Structures*, 230, p.111515.
- AlKhateab, B., Tabrizi, I.E., Zanjani, J.S.M., Rahimi, M.N., Poudeh, L.H., Kefal, A., & Yildiz, M., 2020. Damage mechanisms in CFRP/HNT laminates under flexural and in-plane shear loadings using experimental and numerical

- methods. *Composites Part A: Applied Science and Manufacturing*, 136, p.105962.
- Bruno, R., Toomarian, N., & Salama, M., 1994. Shape estimation from incomplete measurements: a neural-net approach. *Smart Materials and Structures*, 3(2), p.92.
- Cerracchio, P., Gherlone, M., Di Sciuva, M., & Tessler, A., 2015. A novel approach for displacement and stress monitoring of sandwich structures based on the inverse finite element method. *Composite Structures*, 127, 69-76.
- Colombo, L., Sbarufatti, C., & Giglio, M., 2019. Definition of a load adaptive baseline by inverse finite element method for structural damage identification. *Mechanical Systems and Signal Processing*, 120, 584-607.
- Colombo, L., Oboe, D., Sbarufatti, C., Cadini, F., Russo, S., & Giglio, M., 2021. Shape sensing and damage identification with iFEM on a composite structure subjected to impact damage and non-trivial boundary conditions. *Mechanical Systems and Signal Processing*, 148, p. 107163.
- Esposito, M., & Gherlone, M., 2020. Composite wing box deformed-shape reconstruction based on measured strains: Optimization and comparison of existing approaches. *Aerospace Science and Technology*, 99, p. 105758.
- Glaser, R., Caccese, V., & Shahinpoor, M., 2012. Shape monitoring of a beam structure from measured strain or curvature. *Experimental Mechanics*, 52(6), 591-606.
- Gherlone, M., Cerracchio, P., & Mattone, M., 2018. Shape sensing methods: Review and experimental comparison on a wing-shaped plate. *Progress in Aerospace Sciences*, 99, 14-26.
- Kefal, A., Oterkus, E., Tessler, A., & Spangler, J. L., 2016. A quadrilateral inverse-shell element with drilling degrees of freedom for shape sensing and structural health monitoring. *Engineering Science and Technology, an International Journal*, 19, 1299-1313.
- Kefal, A., & Oterkus, E., 2016. Displacement and stress monitoring of a Panamax containership using inverse finite element method. *Ocean Engineering*, 119, 16-29.
- Kefal, A., Tessler, A., & Oterkus, E., 2017. An enhanced inverse finite element method for displacement and stress monitoring of multilayered composite and sandwich structures. *Composite Structures*, 179, 514-540.
- Kefal, A., 2017. Structural health monitoring of marine structures by using inverse finite element method. *PhD Thesis, The University of Strathclyde, Glasgow, UK.*
- Kefal, A., & Yildiz, M., 2017. Modeling of Sensor Placement Strategy for Shape Sensing and Structural Health Monitoring of a Wing-Shaped Sandwich Panel Using Inverse Finite Element Method. *Sensors*, 17(12), 2775.
- Kefal, A., Mayang, J.B., Oterkus, E., & Yildiz, M., 2018. Three dimensional shape and stress monitoring of bulk carriers based on iFEM methodology. *Ocean Engineering*, 147, 256-267.
- Kefal, A., 2019. An efficient curved inverse-shell element for shape sensing and structural health monitoring of cylindrical marine structures. *Ocean Engineering*, 188, p. 106262.
- Kefal, A., Tabrizi, I.E., Tansan, M., Kisa, E., & Yildiz, M., 2021a. An experimental implementation of inverse finite element method for real-time shape and strain sensing of composite and sandwich structures. *Composite Structures*, 258, p. 113431.
- Kefal, A., Tabrizi, I.E., Yildiz, M., & Tessler, A., 2021b. A smoothed iFEM approach for efficient shape-sensing applications: Numerical and experimental validation on composite structures. *Mechanical Systems and Signal Processing*, 152, p. 107486.
- Khan, R.M.A., Tabrizi, I.E., Ali, H.Q., Demir, E., & Yildiz, M., 2020. Investigation on interlaminar delamination tendency of multidirectional carbon fiber composites. *Polymer Testing*, 90, p.106653.
- Kim, N. S., & Cho, N. S., 2004. Estimating deflection of a simple beam model using fiber optic Bragg-grating sensors. *Experimental Mechanics*, 44(4), 433-439.
- Ko, W.L., Richards, W.L., & Fleischer, V.T., 2009. Applications of Ko displacement theory to the deformed shape predictions of the doubly-tapered Ikhana Wing. NASA/TP-2009-214652.
- Li, M.Y., Kefal, A., Cerik, B., & Oterkus, E., 2019. Structural health monitoring of submarine pressure hull using inverse finite element method. In J. Parunov and C. Guedes Soares (Eds.), *Trends in the Analysis and Design of Marine Structures*, 293-299.
- Li, M., Kefal, A., Cerik, B.C., & Oterkus, E., 2020a. Dent damage identification in stiffened cylindrical structures using inverse finite element method. *Ocean Engineering*, 198, p. 106944.
- Li, M., Kefal, A., Oterkus, E., & Oterkus, S., 2020b. Structural health monitoring of an offshore wind turbine tower using iFEM methodology. *Ocean Engineering*, 204, p. 107291.
- Massarwa, E., Tabrizi, I.E., & Yildiz, M., 2021. Mechanical behavior and failure of glass/carbon fiber hybrid composites: Multiscale computational predictions validated by experiments. *Composite Structures*, 260, p.113499.
- Moreira, L., & Soares, C.G., 2020. Neural network model for estimation of hull bending moment and shear force of ships in waves. *Ocean Engineering*, 206, p.107347.
- Oboe, D., Colombo, L., Sbarufatti, C., & Giglio, M., 2021. Shape sensing of a complex aeronautical structure with inverse finite element method. *Sensors*, 21(4), p. 1388.
- Roy, R., Gherlone, M., Surace, C., & Tessler, A., 2021. Full-field strain reconstruction using uniaxial strain measurements: Application to damage detection. *Applied Sciences*, 11(4), p. 1681.
- Silva-Muñoz, R.A., & Lopez-Anido, R.A., 2009. Structural health monitoring of marine composite structural joints using embedded fiber Bragg grating strain sensors. *Composite Structures*, 89(2), 224-234.
- Tabrizi, I.E., Kefal, A., Zanjani, J.S.M., Akalin, C., & Yildiz, M., 2019a. Experimental and numerical investigation on fracture behavior of glass/carbon fiber hybrid composites using acoustic emission method and refined zigzag theory. *Composite Structures*, 223, p. 110971.
- Tabrizi, I.E., Khan, R.M.A., Massarwa, E., Zanjani, J.S.M., Ali, H.Q., Demir, E., & Yildiz, M., 2019b. Determining tab material for tensile test of CFRP laminates with combined usage of digital image correlation and acoustic emission techniques. *Composites Part A: Applied Science and Manufacturing*, 127, p.105623.
- Tessler, A., Riggs, H.R., & Dambach, M., 1999. A novel four-node quadrilateral smoothing element for stress enhancement and error estimation. *International Journal for Numerical Methods in Engineering*, 44(10), 1527-1543.
- Tessler, A., & Spangler, J.L., 2004. Inverse FEM for full-field reconstruction of elastic deformations in shear deformable plates and shells. In: *Proceedings of 2nd European Workshop on Structural Health Monitoring*, Munich, Germany.
- Tessler, A., & Spangler, J. L., 2005. A least-squares variational method for full-field reconstruction of elastic deformations in shear-deformable plates and shells. *Computer Methods in Applied Mechanics and Engineering*, 194(2), 327-339.
- Tessler, A., Di Sciuva, M., & Gherlone, M., 2010. A consistent refinement of first-order shear deformation theory for laminated composite and sandwich plates using improved zigzag kinematics. *Journal of Mechanics of Materials and Structures*, 5(2), 341-367.
- Zhao, F., Bao, H., Liu, J., & Li, K., 2021. Shape sensing of multilayered composite and sandwich beams based on Refined Zigzag Theory and inverse finite element method. *Composite Structures*, 261, p.113321.